Highly Efficient Second-Harmonic Generation of Ultra-Intense Nd:Glass Laser Pulses

Major advances in laser technology at LLE have included the demonstration of high-efficiency frequency doubling and tripling of fusion lasers[1] and the development of short-pulse, chirped-pulse-amplification (CPA) lasers.[2] These technologies were combined a few years ago with the demonstration of 75% efficient frequency doubling of 1.6-ps laser pulses on the CPA T^3 (table-top terawatt) system at LLE, in collaboration with the Australian National University (ANU).[3] Excellent agreement with simulations demonstrated that "standard" frequency conversion theory also applies in the picosecond regime, at intensities up to a few GW/cm^2.

This article reports a more recent collaboration with the University of Michigan. In an extensive series of experiments, 500-fs, 1053-nm laser pulses were converted to the second harmonic in KDP crystals at intensities up to 400 GW/cm^2, with efficiencies of ~80%, without any obvious damage to the crystals. This result extends the regime of validity of the theory nearly two orders of magnitude higher in intensity. Further, the results provide evidence that, at these intensities, it is necessary to include self- and cross-phase modulation in the theory. Most significant, though, may be the extension of the available wavelength range of CPA systems used for ultra-intense laser-matter interaction experiments.

CPA lasers have been successfully used to generate peak laser powers in the infrared well beyond the terawatt regime.[4–7] When focused, these lasers can produce intensities exceeding 10^{18} W/cm^2, giving access to new regimes of laser-matter interaction. For solid targets irradiated at these intensities the peak-to-background intensity contrast of the laser pulse should exceed ~10^9:1 to avoid energy deposition in a plasma created by a much longer prepulse. Second-harmonic generation (SHG) in nonlinear crystals is thus important because, aside from extending the available wavelength range, it significantly improves the contrast ratio. Indeed, high-contrast, second-harmonic laser pulses have been used to produce high-density, high-temperature plasmas that emit short x-ray pulses in the keV region.[8]

The experiments reported here were carried out on a terawatt Nd:glass laser system.[5] In these experiments the laser delivered energies up to 1.5 J with a wavelength of 1.053 μm and a temporal full-width at half-maximum (FWHM) of 500 fs. The spatial profile was somewhat flatter than Gaussian with a diameter of 2.6 cm (FWHM). The intensity contrast ratio was 10^6:1, as measured with a third-order correlator. The pulse energies of the fundamental and its second harmonic were monitored by calorimeters. Three crystal configurations were examined: (a) a type-I crystal, optimum for the SHG of ultrashort 1-μm pulses because the fundamental and second-harmonic group velocities are, for this wavelength, almost equal; (b) a type-II crystal, limited by temporal walkoff between the fundamental o and e pulses; and (c) a predelay scheme using two type-II crystals,[9] in which compensation of this walkoff leads to improved efficiency, as was demonstrated in the collaborative experiments on T^3 with the ANU,[3] and second-harmonic pulse shortening.[10] Results from the current experiments have included high conversion from the type-I crystal (70%–80% throughout the range of 100 to 400 GW/cm^2) and evidence of pulse shortening (to ~100-fs FWHM) from the predelay scheme.

These experiments have been simulated with the LLE code *MIXER*,[11] enhanced to model group-velocity dispersion and $\chi^{(3)}$ effects. The code integrates equations of the form

$$\frac{\partial E_3}{\partial z}+\frac{1}{V_{g3}}\frac{\partial E_3}{\partial t} = -\frac{1}{2}\gamma_3 E_3 - iK_3E_1E_2\exp(i\Delta k\cdot z)$$

$$+i\left\{\alpha_{31}\left|E_1^2\right|+\alpha_{32}\left|E_2^2\right|+\alpha_{33}\left|E_3^2\right|\right\}E_3\,, \quad (1)$$

where, for wave i (waves 1 and 2 combining to generate wave 3), E_i is the electric field, V_{gi} is the group velocity, γ_i is the linear absorption coefficient, K_i is a nonlinear coefficient, and α_{ij} gives the change of refractive index due to the intensity of wave j [resulting from the third-order susceptibility tensor

$\chi^{(3)}$]. The quantity Δk is the wave-vector mismatch, z indicates propagation distance, and t denotes time. The coefficients α_{ij} are related to the more convenient coefficients γ_{ij} defined via the equation $n_i = n_{io} + \Sigma\gamma_{ij}I_j$, which gives the refractive index n_i of wave i in terms of its linear index n_{io} and a nonlinear correction summed over the intensities I_j of waves j. For an isotropic medium and in the absence of dispersion, $\gamma_{ij} = \gamma_0$ for $i = j$ (self-phase modulation); for $i \neq j$ (cross-phase modulation), $\gamma_{ij} = 2\gamma_0$ if the polarizations of waves i and j are parallel and $2\gamma_0/3$ if they are perpendicular.[12] The simulations have used $\gamma_0 = 0.27 \times 10^{-19}$ m^2/W at 1 μm.[13] Since no data is available for 0.5 μm, *MIXER* has used an *ad hoc* model where γ_{ij} is multiplied by a dispersion factor $F \equiv 1.5$ if both waves are second harmonic and $F^{1/2}$ if one is. The propagation and K_3 terms of Eq. (1) are solved in the frequency domain and the $\chi^{(3)}$ term in the time domain. (In the frequency domain, the group-velocity term is replaced by the simple translation of each Fourier mode with its phase velocity, thus including all orders of dispersion.) Predictions for the experimental energy-conversion efficiencies are obtained by averaging solutions to Eq. (1) over the measured two-dimensional spatial profile of the IR laser beam.

Results for the first experiment, doubling in a 4-mm, type-I crystal, are shown in Fig. 60.1(a). Conversion efficiencies of 70%–80% were found from 100 to 400 GW/cm^2, with consistency between the two data sets (from different crystals used five months apart). The nominal intensity plotted on the horizontal axis is close to the intensity in the center of the beam at the peak of the pulse. The beam was modeled as a bandwidth-limited Gaussian of FWHM 500 fs, consistent with experimental spectra and autocorrelations.

Agreement with the simulation for both $\chi^{(3)}$ and $\Delta\theta_1 = 0$ (dashed curve) is generally reasonable, except for a falloff at high intensities ($\gtrsim$100 GW/cm^2). One plausible explanation is nonlinear $\chi^{(3)}$-induced mismatch,[14] modeled here with the solid curves for various angular detunings $\Delta\theta_1$ from small-signal phase matching, measured outside the crystal, with positive $\Delta\theta_1$ indicating an increase in the angle between the propagation direction and the optic axis. The curve labeled $\Delta\theta_1 = 0$ would be followed if the small-signal tuning were sufficiently accurate to locate this direction. However, it was found necessary to fine tune the crystal at high intensity, and it is thus possible that one data set followed $\Delta\theta_1 \approx 0.5$–$0.7$ mrad and the other 0.3 mrad. Dispersion in the (unknown) γ_{ij} coefficients is critical to this explanation. Without dispersion ($F = 1$), the simulations do not depart significantly from the $\chi^{(3)} = 0$ curve even with γ_0 five times bigger; moreover, with

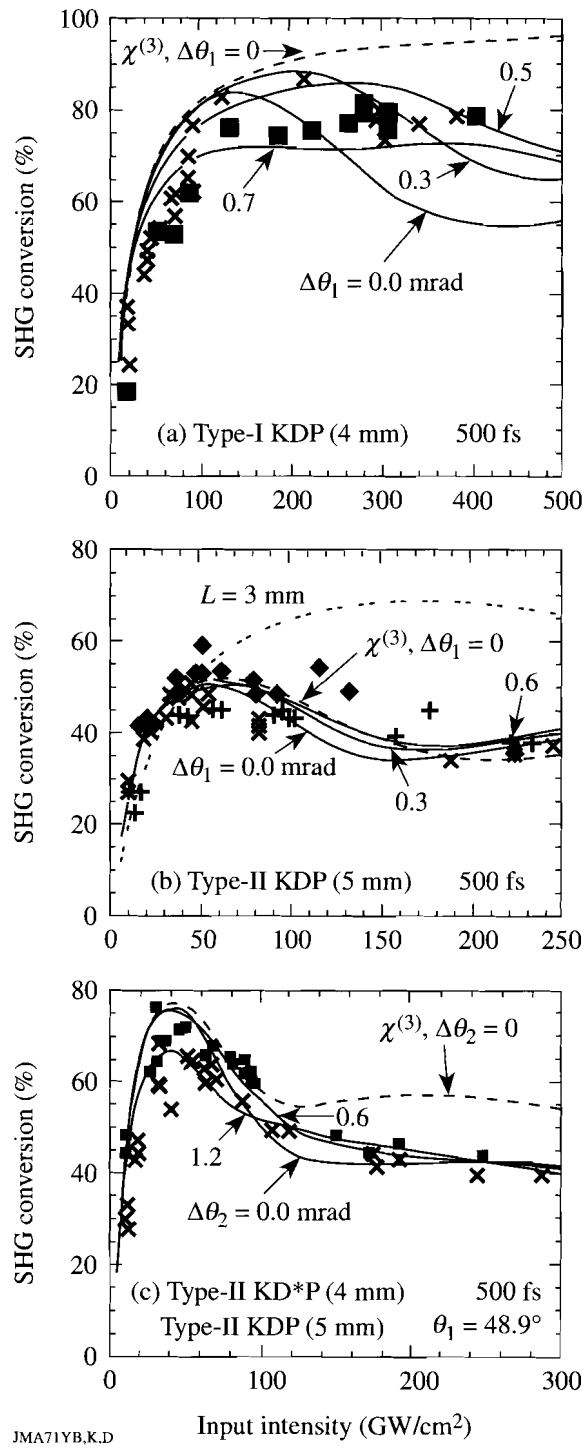

Figure 60.1
SHG efficiency as a function of input laser intensity for (a) a 4-mm, type-I KDP crystal; (b) a 5-mm, type-II KDP crystal; and (c) a 4-mm, detuned, type-II KD*P crystal followed by a 5-mm, type-II KDP crystal. Dashed curves: simulations for $\chi^{(3)} = 0$ and no detuning. Solid curves: simulations including $\chi^{(3)}$ with various angle detunings (in mrad away from the optic axis). The double-dotted curve in (b) is for a 3-mm crystal with $\chi^{(3)} = 0$.

more dispersion ($F = 2$), the simulations fall below the data at 400 GW/cm^2 for all $\Delta\theta_1$. It is worth noting that for any single intensity a $\Delta\theta_1$ can be chosen to fully compensate for the nonlinear phase error,[15] but it is impossible to simultaneously compensate for the full range of intensities in the beam in space and time.

Results for a single, 5-mm-thick, type-II crystal are shown in Fig. 60.1(b) for three data sets. Conversion efficiencies reach 50% at 50 GW/cm^2 and then fall off due to group-velocity walkoff between the fundamental *o* and *e* waves. [This causes incorrect photon ratios (deviating from 1:1) leading to reconversion.] This crystal is much less sensitive to mismatch than the type-I crystal, and the inclusion of $\chi^{(3)}$ terms thus makes little difference. The reconversion seen above 60 GW/cm^2 indicates that the crystal was too thick: the double-dotted curve shows that a 3-mm crystal would perform much better at the higher intensities. Thus, a type-I crystal has just a small advantage at 500 fs. For shorter pulses, however, it is strongly preferred: at 100 fs and comparable intensities the predicted loss is insignificant for type I but catastrophic for type II.

In the third experiment the 5-mm, type-II KDP crystal was preceded by a 4-mm, type-II KD*P crystal, detuned several degrees from phase matching, that provided a predelay between the fundamental *o* and *e* rays. Since the sign of the detuning was unknown, it was assumed that the propagation angle within the KD*P was $\theta_1 = 48.9°$, giving a predelay of 340 fs. [Predictions for the other possibility ($\theta_1 = 58.3°$, predelay = 430 fs) are similar.] Results are shown in Fig. 60.1(c) for experiments carried out on two separate days. Within the data scatter, all curves provide a reasonable fit to the data below ~100 GW/cm^2. At higher intensities, however, the data fall significantly below the prediction for $\chi^{(3)} = 0$ and lie much closer to the curves including $\chi^{(3)}$. As with the type-I case, there is an optimum positive detuning ($\Delta\theta_2$) of the KDP crystal, although here the sensitivity to $\Delta\theta_2$ is smaller. The role of the $\chi^{(3)}$ terms here is more complicated since phase retardations generated at one time in the pulse affect phase matching at other times due to the various group-velocity walkoffs.

The input polarization angle θ_p (the angle of the input electric field vector to the *o* direction of the first crystal[11]) was controlled with a half-wave plate. Two conversion scans carried out as a function of θ_p are shown in Fig. 60.2, one for the single type-II crystal and one for the predelay scheme. Agreement with simulations is generally close, confirming

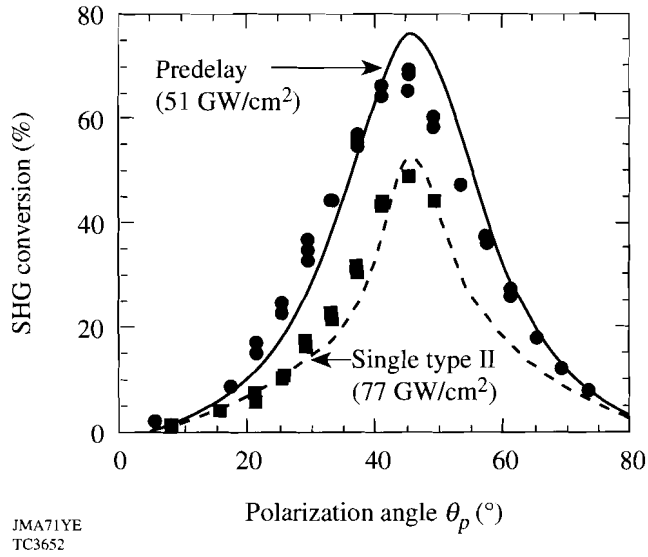

Figure 60.2
Dependence of the SHG efficiency on the polarization angle of the incident laser. Dashed curve: single, 5-mm, type-II KDP crystal at 77 GW/cm^2. Solid curve: predelay scheme at 51 GW/cm^2.

that the polarization state of the laser is substantially correct. The 10% discrepancy at the peak seen for the predelay scheme is consistent with the experimental scatter at the same intensity in Fig. 60.1(c).

The pulse shape of the second harmonic generated by the predelay scheme using a single-shot autocorrelator has been investigated.[16] A portion of the second harmonic was split into two beams that were downcollimated and passed through a 100-μm-thick BBO crystal, incident at angles ±10° to the crystal normal and timed such that the autocorrelation sampled the center of the beam. An experimental fourth-harmonic trace is shown in Fig. 60.3(a) for an estimated IR intensity of 119 GW/cm^2 in the sampled region together with a prediction, including the same $\chi^{(3)}$ model used in Fig. 60.1, for $\Delta\theta_2$ = 1.8 mrad (the optimum detuning at this intensity). The match is very close, except in the wings where the asymmetry is probably explained by spatial intensity variations in the beam. The predicted second-harmonic pulse shape generated by the KDP crystal [Fig. 60.3(b)] shows a narrow central spike with an intensity FWHM of 84 fs, superposed upon a broader wing at the ~15% intensity level. [With $\chi^{(3)} = 0$, a 49-fs FWHM is predicted.] The autocorrelation calculation included propagation through 1.5 cm of BK7 glass (which significantly broadened the pulse to 166-fs FWHM) and group-velocity dispersion within the BBO. It should be cautioned that the 1.8-mrad detuning was not measured but was chosen to illustrate a possible temporal pulse shape consistent with the measured

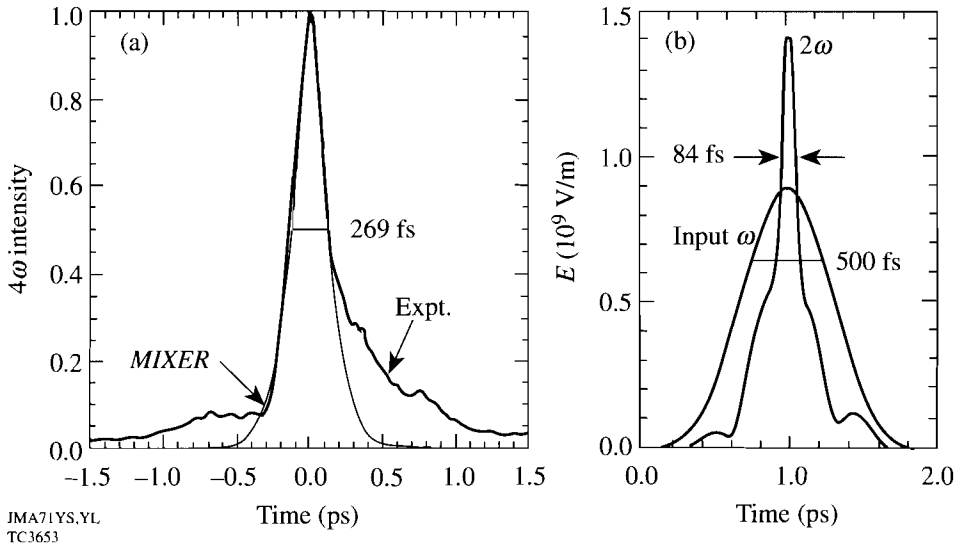

Figure 60.3
(a) Experimental and simulated second-harmonic autocorrelation intensity for the predelay scheme at 119 GW/cm^2. The simulation includes $\chi^{(3)}$ effects and assumes a detuning of 1.8 mrad. (b) Simulated second-harmonic pulse shape at the output of the KDP crystal (electric field versus time).

autocorrelation. Moreover, above ~100 GW/cm^2, structure was generated in the second-harmonic beam that limited its focusability, and the second-harmonic spectrum was broader than predicted with the $\chi^{(3)}$ model. The first demonstration of pulse shortening using the predelay scheme[10] (1.2 ps to 250 fs at 7 GW/cm^2) was unlikely to have been affected by $\chi^{(3)}$ terms.

In conclusion, an extensive series of SHG experiments have been conducted using intense, 500-fs laser pulses. Efficiencies of 70%–80% up to 400 GW/cm^2 were obtained from a type-I crystal without any obvious damage to the crystal or degradation of focusability. Lower efficiencies were obtained for a type-II crystal. The results for the predelay scheme were consistent with a pulse shortening to ≲100-fs FWHM, although with low contrast. All results are broadly in agreement with predictions of the code *MIXER*, with improved agreement obtained above ~100 GW/cm^2 by including a $\chi^{(3)}$ model that makes *ad hoc* assumptions about the dispersion of the self- and cross-phase-modulation coefficients. Further experiments are needed to measure these unknown coefficients. The most important practical consequence of the experiments reported here may be the extension of ultra-intense laser-matter experiments to shorter wavelengths.

ACKNOWLEDGMENT

These experiments were carried out at the University of Michigan by Drs. C. Y. Chien, G. Korn, J. S. Coe, J. Squier, and G. Mourou. This work was supported by the National Science Foundation through the Center for Ultrafast Optical Science under STC PHY 8920108 and by the U.S. Department of Energy Office of Inertial Confinement Fusion under Cooperative Agreement No. DE-FC03-92SF19460, the University of Rochester, and the New York State Energy Research and Development Authority. The support of DOE does not constitute an endorsement by DOE of the views expressed in this article.

REFERENCES

1. W. Seka, S. D. Jacobs, J. E. Rizzo, R. Boni, and R. S. Craxton, Opt. Commun. **34**, 469 (1980).
2. D. Strickland and G. Mourou, Opt. Commun. **56**, 219 (1985).
3. Y. Wang, B. Luther-Davies, Y.-H. Chuang, R. S. Craxton, and D. D. Meyerhofer, Opt. Lett. **16**, 1862 (1991).
4. F. G. Patterson, R. Gonzales, and M. D. Perry, Opt. Lett. **16**, 1107 (1991).
5. Y. Beaudoin *et al.*, Opt. Lett. **17**, 865 (1992).
6. G. Rouyer *et al.*, Opt. Lett. **18**, 214 (1993).
7. C. N. Danson *et al.*, Opt. Commun. **103**, 392 (1993).
8. C. Y. Chien *et al.*, Opt. Lett. **18**, 1535 (1993).
9. Y. Wang and R. Dragila, Phys. Rev. A **41**, 5645 (1990).
10. Y. Wang and B. Luther-Davies, Opt. Lett. **17**, 1459 (1992).
11. R. S. Craxton, IEEE J. Quantum Electron. **QE-17**, 1771 (1981).
12. G. P. Agrawal, *Nonlinear Fiber Optics* (Academic Press, San Diego, 1989).
13. D. Milam and M. Weber, Opt. Commun. **18**, 172 (1976).
14. L. S. Telegin and A. S. Chirkin, Sov. J. Quantum Electron. **12**, 1354 (1982).
15. C. J. McKinstrie and X. D. Cao, J. Opt. Soc. Am. B **10**, 898 (1993).
16. F. Salin, P. Georges, G. Roger, and A. Brun, Appl. Opt. **26**, 4528 (1987).